Gaussianity of Degree-Scale Cosmic Microwave Background Anisotropy Observations

Chan-Gyung Park[1], Changbom Park[1], Bharat Ratra[2], and Max Tegmark[3]

ABSTRACT

We present results from a first test of the Gaussianity of degree-scale cosmic microwave background (CMB) anisotropy. We investigate Gaussianity of the CMB anisotropy by studying the topology of CMB anisotropy maps from the QMAP and Saskatoon experiments. We also study the QMASK map, a combination map of the QMAP and Saskatoon data. We measure the genus from noise-suppressed Wiener-filtered maps at an angular scale of about $1°\!.5$. To test the Gaussianity of the observed anisotropy, we compare these results to those derived from a collection of simulated maps for each experiment in a Gaussian spatially-flat cosmological constant dominated cold dark matter model. The genus-threshold level relations of the QMAP and Saskatoon maps are consistent with Gaussianity. While the combination QMASK map has a mildly non-Gaussian genus curve which is not a consequence of known foreground contamination, this result is not statistically significant at the $2\,\sigma$ level. These results extend previous upper limits on the non-Gaussianity of the large angular scale ($> 10°$) CMB anisotropy (measured by the COBE DMR experiment) down to degree angular scales.

Subject headings: cosmology: observation — cosmic microwave background: anisotropy, topology

1.   Introduction

An important feature of the simplest inflation models is that the initial density fluctuation field has a Gaussian random phase distribution (see, e.g., Fischler, Ratra, & Susskind 1985). Therefore, an observational test of the Gaussianity of the initial density fluctuation field will provide an important constraint on inflation models. Since the CMB temperature anisotropy fluctuation

---

[1]Department of Astronomy, Seoul National University, 151-742 Korea; parkc@astro.snu.ac.kr, cbp@astro.snu.ac.kr.

[2]Department of Physics, Kansas State University, Manhattan, KS 66506; ratra@phys.ksu.edu.

[3]Department of Physics, University of Pennsylvania, Philadelphia, PA 19104; max@physics.upenn.edu.

reflects the density distribution on the last scattering surface, one can study the Gaussianity of the primordial density fluctuation field by measuring the topology of the CMB anisotropy.

Topology measures for two-dimensional fields, introduced by Coles & Barrow (1987), Melott et al. (1989), and Gott et al. (1990), have been applied to many different kinds of observational data. These include the angular distribution of galaxies on the sky (Coles & Plionis 1991; Gott et al. 1992), the distribution of galaxies in slices of the universe (Park et al. 1992; Colley 1997; Park, Gott, & Choi 2001), and the CMB temperature anisotropy field (Coles 1988; Gott et al. 1990; Smoot et al. 1994; Kogut et al. 1996; Colley, Gott, & Park 1996).

Recently, there have been many analyses of the Gaussianity of the CMB anisotropy at large ($> 10°$) angular scales that make use of the DMR maps (Colley et al. 1996; Kogut et al. 1996; Ferreira, Magueijo, & Górski 1998; Novikov, Feldman, & Shandarin 1999; Pando, Valls-Gabaud, & Fang 1998; Bromley & Tegmark 1999; Banday, Zaroubi, & Górski 2000; Magueijo 2000; Mukherjee, Hobson, & Lasenby 2000; Barreiro et al. 2000; Aghanim, Forni, & Bouchet 2001; Phillips & Kogut 2001). While it has been argued that the DMR data shows slight evidence for non-Gaussianity, this has been attributed to non-CMB anisotropy systematics.

Previous studies of the Gaussianity of the CMB anisotropy have been limited to large angular scales, in particular to the DMR maps. On these large angular scales the central limit theorem, in conjunction with sufficient smoothing, ensures that any reasonable theoretical model will predict a Gaussian CMB anisotropy. This does not hold on smaller angular scales. Therefore, it is important to investigate the Gaussianity of the CMB anisotropy on smaller angular scales.

Small-scale CMB anisotropy observations will soon be able to tightly constrain cosmological parameters; see, e.g., Rocha (1999), Page (1999), and Gawiser & Silk (2000) for reviews. Current observational error bars are asymmetric (i.e., non-Gaussian), so accurate constraints on cosmological parameters can only be derived from a complete maximum likelihood analysis of current data (see, e.g., Ganga et al. 1997; Górski et al. 1998; Ratra et al. 1999a; Rocha et al. 1999) or good approximations thereof (Bond, Jaffe, & Knox 2000), although even in this case one assumes that the underlying theoretical model is Gaussian, and it is important to explicitly test this assumption[4]. Derivation of tight constraints on cosmological parameters requires a combined analysis of as many CMB anisotropy data sets as possible. For current data this requires a full maximum likelihood analysis (see, e.g., Ratra et al. 1999b). If the CMB anisotropy is Gaussian and future observational error bars are symmetric (i.e., consistent with Gaussianity), then a χ^2 comparison of CMB anisotropy observations and model predictions will be a much faster way of determining constraints on cosmological parameters (see, e.g., Ganga, Ratra, & Sugiyama 1996; Dodelson & Knox 2000; Tegmark & Zaldarriaga 2000; Le Dour et al. 2000).

---

[4]In fact, comparison of results from different experiments indicates evidence for non-Gaussianity (Podariu et al. 2001), but this is almost certainly a consequence of underestimated observational error bars rather than evidence for a non-Gaussian CMB anisotropy.

In this paper we present results from a first test of the Gaussianity of the small-scale (degree-scale) CMB anisotropy. We measure the genus statistic from CMB anisotropy maps of the QMAP and Saskatoon experiments (which have an angular resolution of about 1° FWHM). We also analyze a combination map of the data from these two experiments (QMASK, Xu et al. 2001). In the next section we summarize the Wiener-filtering method used to construct noise-reduced CMB anisotropy maps and the method used to generate mock simulated survey maps. In §3 we compute the genus of the Wiener-filtered QMAP, Saskatoon, and QMASK maps. Our results are summarized and discussed in §4 and we conclude in §5.

2.   Summary of Map-Making Processes

2.1.   Wiener-filtered maps

The QMAP (balloon-borne) and Saskatoon (ground-based) experiments were designed to measure the degree-scale CMB anisotropy in regions around the north celestial pole (NCP). QMAP measured in the Ka (~ 30 GHz) and Q (~ 40 GHz) bands, with six detectors in two polarizations (Ka1/2, Q1/2, Q3/4), with angular resolutions of 0°.89, 0°.66, and 0°.70 FWHM for Ka1/2, Q1/2, and Q3/4, respectively. See Devlin et al. (1998), Herbig et al. (1998), and de Oliveira-Costa et al. (1998) for details of the experiment and the data from the two flights. The Saskatoon experiment measured the CMB anisotropy with an angular resolution of about 1° in the same frequency range as QMAP. See Netterfield et al. (1997) for details of the experiment and the data from three years of observations. Xu et al. (2001) have combined all QMAP data with Saskatoon data into a degree-scale CMB anisotropy map which they call QMASK. This is the largest degree-scale CMB anisotropy map (648 square degrees). It has an angular resolution of 0°.68 FWHM.

The QMAP maps are very noisy, with large noise correlations between pixels. The Saskatoon map is linear combinations of sky temperatures convolved with complicated synthesized beams. Wiener-filtering suppresses the noisiest modes in a map, thus emphasizing a statistically significant signal. Tegmark (1997) reviews the general map-making process and discusses the various filters used. In what follows we summarize our Wiener-filtering of the QMAP data, based on de Oliveira-Costa et al. (1998). We also apply this method to the QMASK data. The Saskatoon data are more complicated and for this we adopt the Wiener-filtering method of Tegmark et al. (1997).

The QMAP data are composed of n-dimensional map vectors X's (the temperature at each of the n pixels) and $n \times n$-dimensional covariance matrices N's which characterize the pixel noise. The numbers of pixels of the QMAP data set are 2695 (1Ka1/2 band), 2754 (1Q2), and 2937 (1Q3/4) for the 1st flight, and 1625 (2Ka1/2), 1633 (2Q1/2), and 1591 (2Q3/4) for the 2nd flight. For the Saskatoon data set the number of data points (sky temperatures convolved with the synthesized beams) are 2586 for the NCP Cap data. The QMASK data, the combined version of QMAP and Saskatoon, has 6495 pixel temperatures.

For each experiment we compute the Wiener-filtered map X_{WF} given by

$$X_{\text{WF}} = S[S + N]^{-1}X. \tag{1}$$

Here S is the CMB theoretical model covariance matrix defined as

$$S_{ij} = \langle X_{\text{CMB}}X_{\text{CMB}}^T \rangle = \sum_{\ell=2}^{\infty} \frac{(2\ell + 1)}{4\pi} P_\ell(\hat{r}_i \cdot \hat{r}_j) B_\ell^2 C_\ell, \tag{2}$$

where we sum over multipole moments ℓ, X_{CMB} is the CMB theoretical model temperature map vector, P_ℓ's are Legendre polynomials, and B_ℓ's are the spherical harmonic expansion coefficients of the beam of the experiment. For QMAP and Saskatoon, the CMB anisotropy theoretical spectrum we use is the flat bandpower spectrum $C_\ell = \frac{24\pi}{5}Q^2/\ell(\ell + 1)$ normalized to $Q = 30$ μK. The global appearance of a map depends on the bandpower at the angular scales where the experiment is sensitive (Tegmark et al. 1997). If we use a different power spectrum for the signal, e.g., a spatially-flat cosmological constant (Λ) dominated cold dark matter (CDM) model power spectrum, the temperatures of the filtered map change, but the overall distribution of hot and cold spots is conserved. The QMASK data contains more cosmological information than QMAP or Saskatoon alone, so we use a flat-Λ CDM model power spectrum (see §2.2) to Wiener-filter QMASK. Such a spectrum more accurately summarizes available CMB anisotropy observations (e.g., Podariu et al. 2001).

The Wiener-filtered maps generally have the same angular resolution as the experimental beams. This is true for the QMAP and QMASK data. That is, these maps have angular resolutions of 0°.89, 0°.66, and 0°.70 FWHM for QMAP Ka1/2, Q1/2, and Q3/4, respectively, and 0°.68 FWHM for QMASK. For Saskatoon, however, there is an additional 1° FWHM smoothing in the filtering process (see Tegmark et al. 1997 for details). Assuming a 1° FWHM angular resolution for the Saskatoon experiment, the total angular resolution of the Saskatoon Wiener-filtered map is approximately 1°.4 FWHM.

To compute the genus we stereographically project the Wiener-filtered maps on to a plane. This projective mapping is conformal and locally preserves shapes of structures. A Gaussian interpolation filter is used in the projection. We choose the radius of the Gaussian filter to be 2.5 times the pixel size, where the pixel sizes are those of the Wiener-filtered maps. The total smoothing scales of the final maps are 1°.53, 1°.6, and 1°.42 FWHM for QMAP, Saskatoon, and QMASK, respectively.

2.2. Mock Survey Maps

We have generated 50 Wiener-filtered mock survey maps for each experiment. To generate these CMB anisotropy maps we use a flat-Λ CDM model spectrum with Λ density parameter $\Omega_\Lambda = 0.6$, non-relativistic matter density parameter $\Omega_0 = 0.4$, $h = 0.6$ (where the Hubble constant

$H_0 = 100h$ km s^{-1} Mpc^{-1}), and baryonic density parameter $\Omega_B = 0.0125h^{-2}$ (Ratra et al. 1997). First the pure CMB anisotropy flat-Λ model map is observed at 50 different parts of the sky using the method of Park et al. (1998). Then the instrumental noise is generated from the noise covariance matrix. The noise map vector of each experiment is computed from $\vec{n} = N^{1/2}\vec{n}_r$ where $N^{1/2}$ is the Cholesky decomposition of the noise covariance matrix and $\vec{n}_r$ is a vector of the same dimension as $\vec{n}$ and is composed of samples randomly drawn from a unit normal distribution (Netterfield et al. 1997, §10).

The 50 pure CMB anisotropy signal map vectors are convolved with the beam of each experiment. They are then added to the instrumental noise map vectors to produce the mock survey data. These CMB mock survey maps are Wiener-filtered and projected stereographically in the same way that the observational data are analyzed. The Wiener-filtered versions of the observed QMAP and Saskatoon CMB maps are shown in Figure 1, along with Wiener-filtered mock maps. The observed QMASK Wiener-filtered map is shown in the Figure 2a together with mock QMASK maps (Fig. 2c and 2d).

3. Genus Analysis

We use the two-dimensional genus statistic introduced by Gott et al. (1990) as a quantitative measure of the topology of the CMB anisotropy. For the two-dimensional CMB anisotropy temperature field the genus is the number of hot spots minus the number of cold spots. Equivalently the genus at a temperature threshold level ν is

$$g(\nu) = \frac{1}{2\pi} \int_C \kappa ds, \tag{3}$$

where κ is the signed curvature of the iso-temperature contours C. The genus curve as a function of the temperature threshold level has a characteristic S shape for a Gaussian random-phase field.

The theoretical genus per steradian of a two-dimensional Gaussian field with correlation function $C(\theta)$ is (Gott et al. 1990)

$$g(\nu) = \frac{1}{(2\pi)^{3/2}} \frac{C^{(2)}}{C^{(0)}} \nu e^{-\nu^2/2}, \tag{4}$$

where $C^{(n)} \equiv (-1)^{n/2}(d^n C/d\theta^n)_{\theta=0}$, and the temperature threshold is $\nu(C^{(0)})^{1/2} = \nu\sigma$. For a CMB anisotropy temperature map convolved with a beam B and a smoothing filter F, the genus per steradian can be expressed in terms of the CMB power spectrum C_ℓ as

$$g(\nu) = \frac{1}{2(2\pi)^{3/2}} \frac{\sum \ell(\ell+1)(2\ell+1)C_\ell B_\ell^2 F_\ell^2}{\sum(2\ell+1)C_\ell B_\ell^2 F_\ell^2} \nu e^{-\nu^2/2}. \tag{5}$$

The genus curve shape is fixed by the Gaussian random-phase nature of the anisotropy field and its amplitude depends only on the shape of C_ℓ and not on its amplitude.

Non-Gaussian features in the CMB anisotropy will affect the genus curve in many different ways. Since the genus-threshold level relation is known for Gaussian fields, non-Gaussian behavior of a field can be detected from deviations of the genus curve from this relation (Park et al. 1998, 2001). Non-Gaussianity can shift the observed genus curve to the left (toward negative thresholds) or right near the mean threshold level. It can also alter the amplitudes of the genus curve at positive and negative levels differently causing $|g(\nu = -1)| \neq |g(\nu = +1)|$. We quantify these properties by using genus-related statistics.

First the shift of the genus curve $\Delta\nu$ (Park et al. 1992, 1998, 2001) is measured from the genus curve by minimizing the χ^2 between the data and the fitting function

$$G = A_s \nu' e^{-\nu'^2/2}, \tag{6}$$

where $\nu' = \nu - \Delta\nu$, and the amplitude A_s of the genus curve is allowed to have different values at negative and positive ν'. The fitting is performed over the range $-1.0 \leq \nu \leq 1.0$. The second statistic is the asymmetry parameter which measures the difference in the amplitude of the genus curve at positive and negative thresholds (i.e., the difference between the numbers of hot and cold spots at positive and negative threshold levels, respectively). The asymmetry parameter is defined as

$$\Delta g = A_H - A_C, \tag{7}$$

where

$$A_H = \int_{\nu_1}^{\nu_2} g_{\mathrm{obs}} d\nu / \int_{\nu_1}^{\nu_2} g_{\mathrm{fit}} d\nu, \tag{8}$$

and likewise for A_C. The integration is limited to $-2.4 \leq \nu \leq -0.4$ for A_C and to $0.4 \leq \nu \leq 2.4$ for A_H. The overall amplitude A of the best-fit Gaussian genus curve g_{fit} is found from χ^2-fitting over the range $-2.4 \leq \nu \leq 2.4$. Positive Δg means that more hot spots are present than cold spots. In summary, for a given genus curve we measure the best-fit amplitude A, the shift parameter $\Delta\nu$, and the asymmetry parameter Δg.

We present the genus curves as a function of the area fraction threshold level ν_A. ν_A is defined to be the temperature threshold level at which the corresponding iso-temperature contour encloses a fraction of the survey area equal to that at the temperature threshold level ν_A for a Gaussian field. The genus estimated at each threshold level is an average over three genus values with threshold levels ν_A shifted by 0 and ±0.1. The amplitude of the genus curves for each band and flight of QMAP are low because of the small survey area. So we have averaged all QMAP genus curves over bands (Ka & Q) and flights (1st & 2nd) to get a total QMAP genus curve.

Figure 3 shows the observed genus curves (filled dots) of the Wiener-filtered versions of the observed QMAP and Saskatoon maps and their best fitting Gaussian genus curves (solid curves). Open circles are the median genus curves from 50 realizations of Wiener-filtered mock survey maps made using the Gaussian flat-Λ CDM model. The error bars are the $\pm68\%$ uncertainty limits from the 50 genus values. The QMASK genus curve is shown in Figure 4a. Table 1 lists the genus-related statistics A, $\Delta\nu$, and Δg (only for QMASK) measured from each CMB map, as well as the results

from the mock survey maps. The 68% uncertainty limits are again estimated from the 50 A, $\Delta\nu$, and Δg values obtained from the mock data.

4. Discussion

The observed genus curves of the QMAP and Saskatoon maps have shift parameters consistent with zero, and are consistent with those of the simulated Gaussian model. Although there are some deviations in the observed genus curves from the Gaussian curves at high threshold levels, i.e., at $\nu_A \gtrsim 2.0$, for both QMAP and Saskatoon, these effects are probably not evidence for non-Gaussianity in the CMB anisotropy but are probably caused by the small areas of the observed fields. This is because the genus is forced to have non-zero values even at high threshold levels when it is given as a function of the area fraction threshold level.

The QMASK genus curve, however, has a different behavior. Its Gaussian fitting curve matches well the mock survey result and the shift parameter $\Delta\nu_{\mathrm{obs}} = +0.18$ is consistent with zero. From the 50 mock survey maps, the probability that the shift parameter $|\Delta\nu| \geq 0.18$ is 20%. In the QMASK Wiener-filtered map there are many fewer hot spots near $\nu_A = +1$ than cold spots near $\nu_A = -1$. This difference in the number of hot and cold spots causes an asymmetry of the genus curve, $\Delta g_{\mathrm{obs}} = -0.37$. The phenomenological reason for this asymmetry is that the observed region of the first flight QMAP experiment in the QMASK map, especially the middle-left region of Figure 2a, has many cold spots near the threshold level $\nu_A = -1$. We now consider a few possibilities which might cause this asymmetry.

The first possibility for the asymmetry in the genus curve is the statistical effect caused by a small survey area. From the 50 genus curves of the mock survey maps, we estimate the probability that a genus curve measured from the QMASK survey area has asymmetry parameter $|\Delta g| \geq 0.37$ to be 18%. Therefore, the asymmetry of QMASK genus curve is not a very significant effect.

The second is the effect of Galactic foreground contamination in the QMASK data since the survey region is located at low Galactic latitude ($8° \lesssim b \lesssim 46°$). De Oliveira-Costa et al. (1997, 2000) have quantified the level of foreground contamination in the QMAP and Saskatoon data by using a cross-correlation technique. For the Saskatoon experiment they detect a marginal correlation with the Diffuse Infrared Background Experiment (DIRBE) maps, but no significant correlation with synchrotron emission maps. They also find that the QMAP 30 GHz Ka-band data are significantly correlated with synchrotron maps but not with the DIRBE maps. However, an overall consideration of the effects of these foreground contaminations on the CMB temperature fluctuations show that the Saskatoon and QMAP data are not seriously contaminated by foreground sources since the foreground signal causes the CMB fluctuations to be overestimated by only a few percent. Because the foreground and CMB temperature fluctuations add in quadrature, a foreground signal with an amplitude a few tens of a percent of the CMB fluctuation will cause the CMB fluctuations to be overestimated by only a few percent.

In this study we investigate the effect of foreground contamination on genus appearance by using the cross-correlation technique of de Oliveira-Costa et al. (2000) to quantify the level of Galactic emission contamination in the QMASK data. The high resolution 100 μm dust map (Schlegel, Finkbeiner, & Davis 1998) and the 1420 MHz synchrotron map (Reich 1982; Reich & Reich 1986) are used as foreground templates. The results, summarized in Table 2, show that the QMASK data are marginally correlated with Galactic foreground emission, especially with synchrotron emission. Here, the coefficients $\hat{a}$'s represent the correlation of foreground templates with the QMASK map and the ΔT's are the corresponding temperature fluctuations ($\Delta T = \hat{a}\sigma_{\mathrm{Gal}}$, where σ_{Gal} is the standard deviation of the template map). The best-fit estimate of the foreground contribution to the QMASK map is obtained by summing the two foreground maps multiplied by the correlation coefficients $\hat{a}$. However, the genus curve measured from the foreground-subtracted QMASK map is also asymmetric (Fig. 4b and Table 1). The asymmetry is somewhat larger ($\Delta g = -0.46$) but the probability that the asymmetry parameter $|\Delta g| \geq 0.46$ is still only 10%. The Wiener-filtered version of the foreground template used in this analysis is shown in Figure 2b. We have also computed the genus of the mock surveys after adding the Galactic foreground template to the mock survey CMB anisotropy maps. Adding the foreground causes negligible asymmetry and shift, compared with the results of the foreground-free mock survey. The genus curve estimated from the QMASK data with a Galactic cut at $b > 20°$ also has essentially the same shape. Thus these foregrounds cannot be responsible for the degree-scale spots. It is most probable that the QMASK survey region has statistically more cold CMB spots and less hot spots.

5. Conclusions

We present results from a first test of the Gaussianity of degree-scale CMB anisotropy. The observed QMAP, Saskatoon, and QMASK CMB anisotropy fields are Gaussian, given the errors. In combination with previous upper limits on the non-Gaussianity of the large-scale (DMR-scale) CMB anisotropy, these results indicate that the CMB anisotropy appears to be Gaussian all the way from angular scales $> 10°$ down to degree angular scales.

Larger area CMB anisotropy maps with higher signal-to-noise will allow for a more confident test of Gaussianity of the degree and sub-degree scale CMB anisotropy. The recent BOOMERanG 1998 and MAXIMA-1 data appear promising for this purpose.

Table 1.   Genus-Related Statistics Measured from the Wiener-Filtered Observed QMAP, Saskatoon, and QMASK Maps

Wiener-Filtered Map	A	$\Delta\nu_{\mathrm{obs}}$	$\Delta\nu_{\mathrm{mock}}$	Δg_{obs}	Δg_{mock}
QMAP	2.51	$+0.11$	$+0.00 \pm 0.10$		
Saskatoon	6.58	-0.04	$+0.00 \pm 0.11$		
QMASK	16.89	$+0.18$	$+0.02 \pm 0.13$	-0.37	-0.02 ± 0.28
QMASK (Foreground Subtracted)	16.78	$+0.16$	$+0.02 \pm 0.13$	-0.46	-0.02 ± 0.28

Table 2.   Correlations between the QMASK Map and Galactic Emissions

Foreground Map	$\hat{a} \pm \Delta\hat{a}$[a]	$\hat{a}/\Delta\hat{a}$	σ_{Gal}[b]	ΔT (μK)[c]
100 μm dust	1.88 ± 4.17	0.45	3.78	7.1 ± 15.8
1420 MHz synchrotron	0.15 ± 0.07	2.01	172.9	25.9 ± 12.1

[a]$\hat{a}$ has the unit of μK(MJy/sr)$^{-1}$ for the 100 μm template, and μK(mK)$^{-1}$ for the 1420 MHz template.

[b]RMS levels in units of the foreground template maps. Units are MJy/sr for the 100 μm dust map, and mK for the 1420 MHz synchrotron emission map.

[c]$\Delta T \equiv (\hat{a} \pm \Delta\hat{a})\sigma_{\mathrm{Gal}}$.

REFERENCES

Aghanim, N., Forni, O., & Bouchet, F.R. 2001, A&A, 365, 341

Banday, A.J., Zaroubi, S. & Górski K.M. 2000, ApJ, 533, 575

Barreiro, R.B., Hobson, M.P., Lasenby, A.N., Banday, A.J., Górski, K.M., & Hinshaw, G. 2000, MNRAS, 318, 475

Bond, J.R., Jaffe, A.H., & Knox, L. 2000, ApJ, 533, 19

Bromley, B.C., & Tegmark, M. 1999, ApJ, 524, L79

Coles, P. 1988, MNRAS, 234, 509

Coles, P., & Barrow, J.D. 1987, MNRAS, 228, 407

Coles, P., & Plionis, M. 1991, MNRAS, 250, 75

Colley, W.N. 1997, ApJ, 489, 471

Colley, W.N., Gott, J.R., & Park, C. 1996, MNRAS, 281, L82

de Oliveira-Costa, A., Devlin, M.J., Herbig, T., Miller, A.D., Netterfield, C.B., Page, L.A., & Tegmark, M. 1998, ApJ, 509, L77

de Oliveira-Costa, A., Kogut, A., Devlin, M.J., Netterfield, C.B., Page, L.A., & Wollack, E.J. 1997, ApJ, 482, L17

de Oliveira-Costa, A., et al. 2000, ApJ, 542, L5

Devlin, M.J., de Oliveira-Costa, A., Herbig, T., Miller, A.D., Netterfield, C.B., Page, L.A., & Tegmark, M. 1998, ApJ, 509, L69

Dodelson, S., & Knox, L. 2000, Phys. Rev. Lett., 84, 3523

Ferreira, P.G., Magueijo, J., & Górski, K.M. 1998, ApJ, 503, L1

Fischler, W., Ratra, B., & Susskind, L. 1985, Nucl. Phys. B, 259, 730

Ganga, K., Ratra, B., Gundersen, J.O., & Sugiyama, N. 1997, ApJ, 484, 7

Ganga, K., Ratra, B., & Sugiyama, N. 1996, ApJ, 461, L61

Gawiser, E., & Silk, J. 2000, Phys. Rept., 333-334, 245

Górski, K.M., Ratra, B., Stompor, R., Sugiyama, N., & Banday, A.J. 1998, ApJS, 114, 1

Gott, J.R., Mao, S., Park, C., & Lahav, O. 1992, ApJ, 385, 26

Gott, J.R., Park, C., Juszkiewicz, R., Bies, W.E., Bennett, D.P., Bouchet, F.R., & Stebbins, A. 1990, ApJ, 352, 1

Herbig, T., de Oliveira-Costa, A., Devlin, M.J., Miller, A.D., Page, L.A., & Tegmark, M. 1998, ApJ, 509, L73

Kogut, A., Banday, A.J., Bennett, C.L., Górski, K.M., Hinshaw, G., Smoot, G.F., & Wright, E.L. 1996, ApJ, 464, L29

Le Dour, M., Douspis, M., Bartlett, J.G., & Blanchard, A. 2000, A&A, submitted

Magueijo, J. 2000, ApJ, 528, L57

Melott, A.L., Cohen, A.P., Hamilton, A.J.S., Gott, J.R., & Weinberg, D.H. 1989, ApJ, 345, 618

Mukherjee, P., Hobson, M.P., & Lasenby, A.N. 2000, MNRAS, 318, 1157

Netterfield, C.B., Devlin, M.J., Jarosik, N., Page, L., & Wollack, E.J. 1997, ApJ, 474, 47

Novikov, D., Feldman, H., & Shandarin, S. 1999, Int. J. Mod. Phys. D, 8, 291

Page, L.A. 1999, astro-ph/9911199

Pando, J., Valls-Gabaud, D., & Fang, L.-Z. 1998, Phys. Rev. Lett., 81, 4568

Park, C., Colley, W.N., Gott, J.R., Ratra, B., Spergel, D.N., & Sugiyama, N. 1998, ApJ, 506, 473

Park, C., Gott, J.R., & Choi, Y.J. 2001, ApJ, in press, astro-ph/0008353

Park, C., Gott, J.R., Melott, A.L., & Karachentsev, I.D. 1992, ApJ, 387, 1

Phillips, N.G., & Kogut, A. 2001, ApJ, 548, 540

Podariu, S., Souradeep, T., Gott, J.R., Ratra, B., & Vogeley, M.S. 2001, astro-ph/0102264

Ratra, B., Ganga, K., Stompor, R., Sugiyama, N., de Bernardis, P., & Górski, K.M. 1999a, ApJ, 510, 11

Ratra, B., Stompor, R., Ganga, K., Rocha, G., Sugiyama, N., & Górski, K.M. 1999b, ApJ, 517, 549

Ratra, B., Sugiyama, N., Banday, A.J., & Górski, K.M. 1997, ApJ, 481, 22

Reich, W. 1982, A&AS, 48, 219

Reich, P., & Reich, W. 1986, A&AS, 63, 205

Rocha, G. 1999, in Dark Matter in Astrophysics and Particle Physics 1998, ed. H.V. Klapdor-Kleingrothaus & L. Baudis (Bristol: Institute of Physics Publishing), 238

Rocha, G., Stompor, R., Ganga, K., Ratra, B., Platt, S.R., Sugiyama, N., & Górski, K.M. 1999, ApJ, 525, 1

Schlegel, D.J., Finkbeiner, D.P., & Davis, M. 1998, ApJ, 500, 525

Smoot, G.F., Tenorio, L., Banday, A.J., Kogut, A., Wright, E.L., Hinshaw, G., & Bennett, C.L. 1994, ApJ, 437, 1

Tegmark, M. 1997, ApJ, 480, L87

Tegmark, M., de Oliveira-Costa, A., Devlin, M.J., Netterfield, C.B., Page, L., & Wollack, E.J., 1997, ApJ, 474, L77

Tegmark, M., & Zaldarriaga, M. 2000, ApJ, 544, 30

Xu, Y., Tegmark, M., de Oliveira-Costa, A., Devlin, M.J., Herbig, T., Miller, A.D., Netterfield, C.B., & Page, L. 2001, Phys. Rev. D, in press, astro-ph/0010552

FIGURE CAPTIONS

Fig. 1.— Wiener-filtered maps for QMAP and Saskatoon CMB anisotropy experiments. The top two rows show the Wiener-filtered observed QMAP maps for each band and flight. Note that the maps are not on the same scale; the second flight maps are magnified by a factor of 2 relative to the first flight maps. The next two rows show one set of the 50 Wiener-filtered mock QMAP survey maps. The Wiener-filtered observed Saskatoon map and two examples of Wiener-filtered mock Saskatoon maps are shown in the bottom row. In all maps R.A. = 0° is at the top and increases clockwise.

Fig. 2.— Wiener-filtered versions of a) the observed QMASK data, b) the Galactic foreground template, and c), d) two examples of mock QMASK maps. The Galactic foreground shown in b), subdominant to the CMB signal, is amplified by a factor of five for ease of visualization. The dotted lines on the QMASK map in a) indicate Galactic latitudes of $b = 10°$, $20°$, and $30°$, from top to bottom.

Fig. 3.— The genus curves (filled dots) measured from the Wiener-filtered observed maps of a) the QMAP and b) Saskatoon CMB anisotropy experiments. The solid lines are Gaussian curves, best fit to the measured genus points. The open circles are the median genus curve of 50 Wiener-filtered mock surveys in a Gaussian flat-Λ CDM cosmological model.
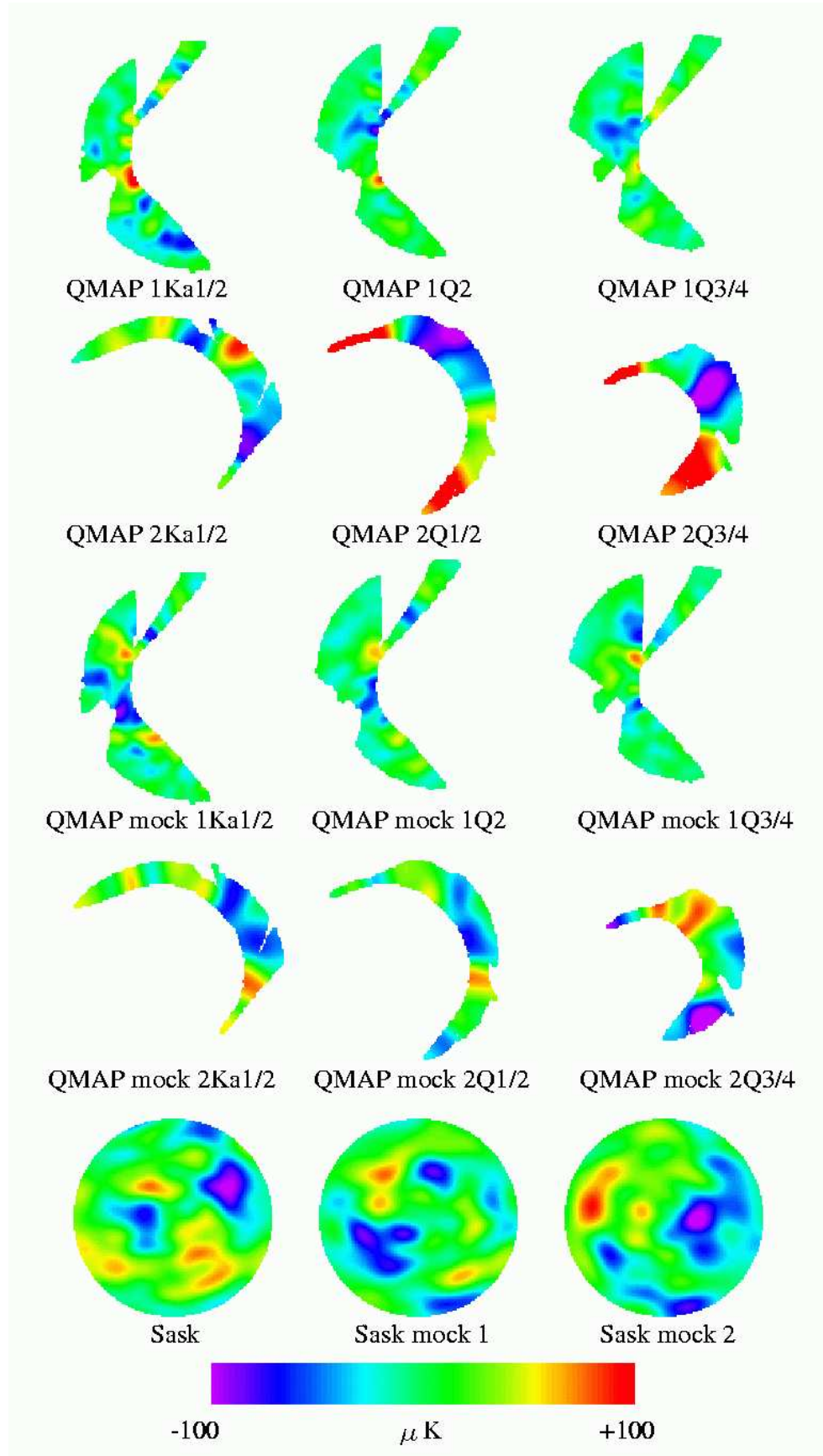
Fig. 4.— The genus curves (filled dots) measured from the Wiener-filtered observed maps of the a) QMASK data and b) QMASK data with known foreground contamination removed. The solid lines are Gaussian curves, best fit to the measured genus points. The open circles are the median genus curve of 50 Wiener-filtered mock QMASK surveys in a Gaussian flat-Λ CDM cosmological model.

Figure 1

(a)

OMASK

(b)

Galactic Foreground
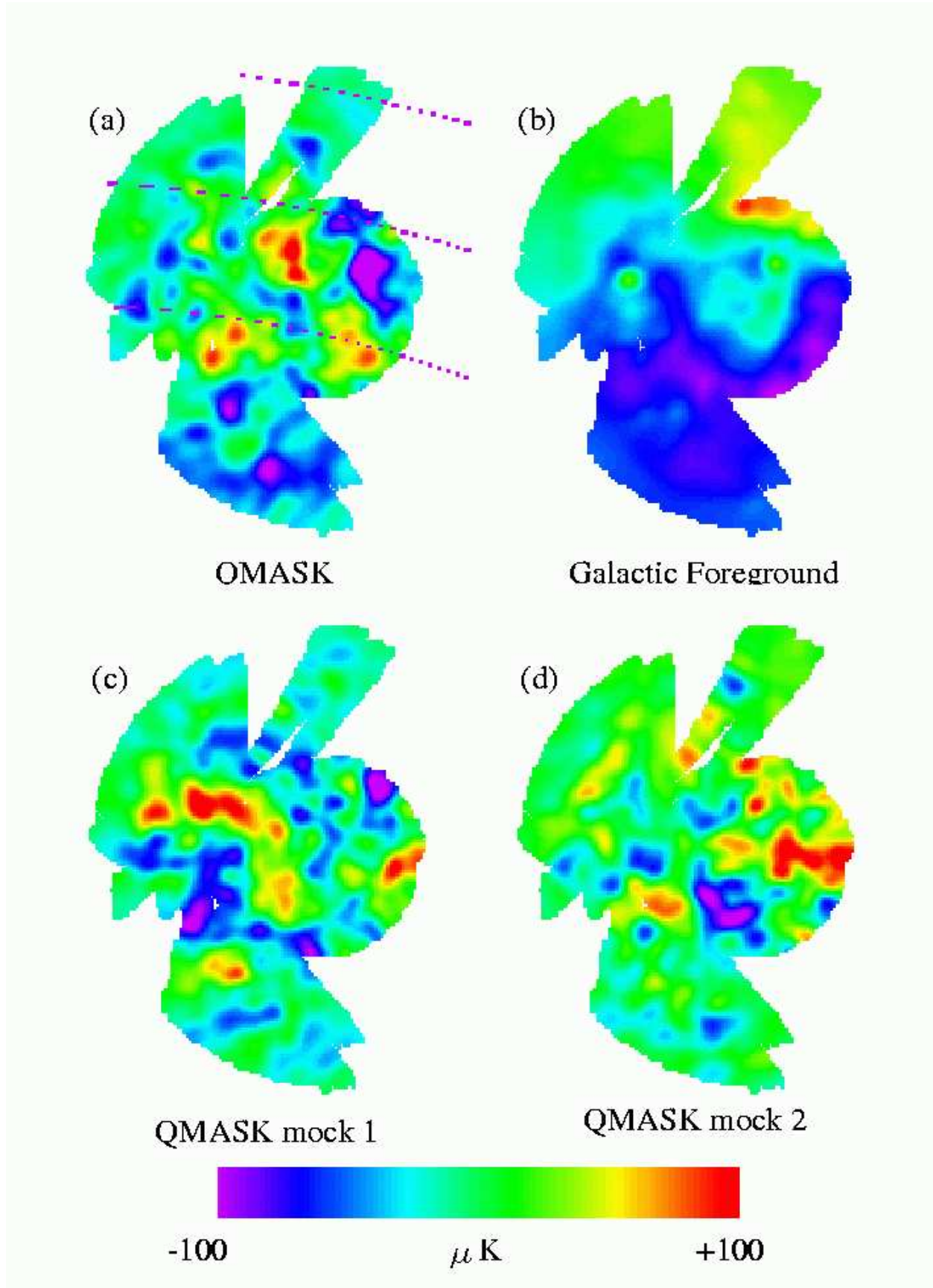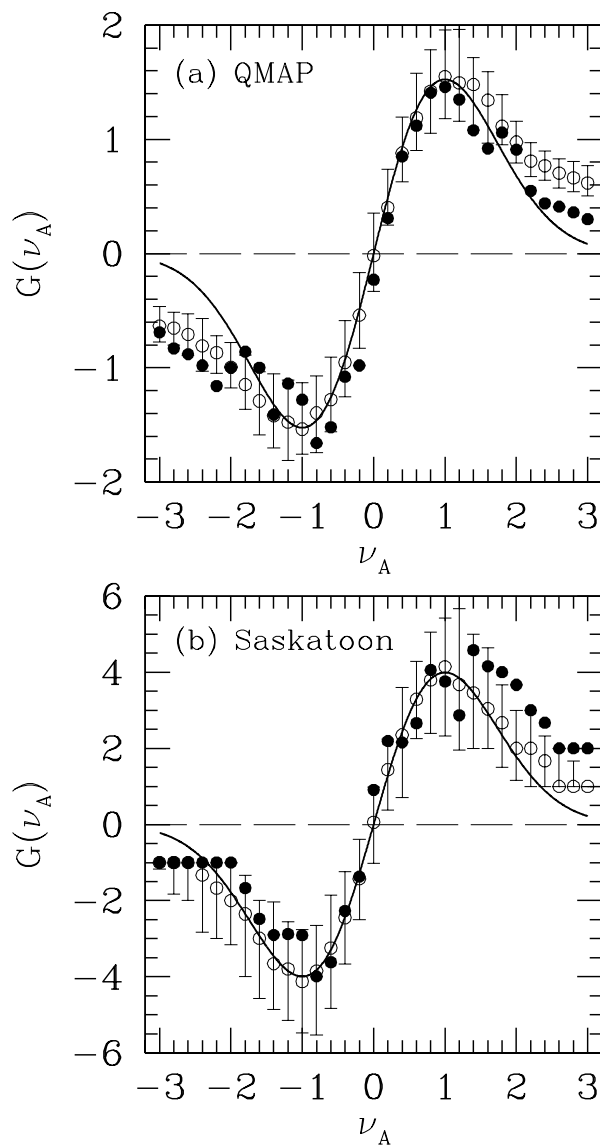
(c)

QMASK mock 1

(d)

QMASK mock 2

-100 μ K   +100

Figure 2

Figure 3

Figure 4